J. Synchrotron Rad. (2000). **7**, 27–33

Simultaneous IR and time-resolved X-ray diffraction measurements for studying self-sustained reactions

F. Bernard,[a]* E. Gaffet,[b] M. Gramond,[c] M. Gailhanou[d] and J. C. Gachon[e]

[a]Laboratoire de Recherches sur la Réactivité des Solides, UMR 5613 CNRS, Université de Bourgogne, BP 47870, F-21078 Dijon CEDEX, France, [b]UPR A0806 CNRS, 'Far from Equilibrium Phase Transitions' Group, F-90010 Belfort CEDEX, France, [c]Laboratoire Chimie Physique du Solide, URA 453 CNRS, Ecole Centrale, F-92295 Chatenay-Malabry, France, [d]LURE (CNRS/CEA), Université de Paris-Sud, F-91400 Orsay, France, and [e]Laboratoire de Chimie du Solide Minéral, UMR 7555 CNRS, Université Henri Poincaré, Nancy 1, BP 239, F-54506 Vandoeuvre les Nancy CEDEX, France. E-mail: fbernard@u-bourgogne.fr

(*Received 20 December 1998; accepted 21 October 1999*)

Self-propagating high-temperature synthesis provides an attractive practical method for producing advanced materials such as ceramics, composites and intermetallics. This kind of reaction has been investigated *in situ* using time-resolved X-ray diffraction, with an X-ray synchrotron beam (D43 beamline, LURE, Orsay) coupled to simultaneous IR thermography to study structural transformations and thermal evolution. With short acquisition times (30 ms per pattern) it has been possible to observe several steps before obtaining compounds. Two different compound formations have been described: (i) the different steps of reaction, aluminium melting, subsequent temperature increase and fast reaction between Al and Ni at such temperatures that only Ni and AlNi are solid and all other compositions are liquid and well identified; (ii) the formation of FeAl. Here, a portion of the iron seems to transform into its allotropic phase and this transition stabilizes the reaction temperature at $\sim$1173 K. In addition, the aluminium melting during the reaction explains why the nanostructure induced by the mechanical activation is maintained in the end product.

Keywords: self-propagating high-temperature synthesis; time-resolved X-ray diffraction; *in situ*; intermetallics; Fe/Al; Ni/Al.

1. Introduction

Combustion synthesis, or self-propagating high-temperature synthesis (SHS) (Merzhanov & Borovinskaya, 1972), provides an attractive practical method for producing advanced materials, such as ceramics, composites and intermetallics. SHS offers advantages with respect to process economy and simplicity. The basis of SHS relies on the ability of highly exothermic reactions to be self-sustaining and, therefore, energetically efficient. If a very exothermic reaction between solid or solid and liquid reactants is locally initiated it may generate enough heat to ensure the propagation of a transformation front throughout all the reactants to yield the product. These processes are characterized by a fast-moving combustion front (1–100 mm s^{-1}) and a self-generating heat which leads to a sharp increase of temperature, sometimes up to several thousand K (Munir, 1988). The temperature reached inside the reaction front may be high enough to volatilize low-boiling-point impurities and therefore help to produce purer products than those obtained by more conventional techniques. At the same time, if the temperature variation after the formation of the product is kept under control, it is possible to avoid the appearance of macrosegregation in the solid. Although basic concepts of this synthesis method seem relatively easy to apply, some fundamental questions concerning the physical and chemical nature of transformations in the reaction front remain unsolved.

Until recently it has been difficult to investigate these reactions by conventional techniques due to the high temperatures involved and the fast rates of combustion. Conventional techniques do not permit the study of the intimate mechanisms which control these reactions, such as the role of liquid formation, the existence and effect of transitory phases and of other parameters which may induce changes to the texture or nature of the end products. Recently, real time *in situ* investigations of structural changes and chemical dynamics in the combustion area have been made possible by the use of synchrotron radiation. Table 1 summarizes the different technical improvements which have been implemented to perform time-resolved X-ray diffraction (TRXRD) studies in the case of self-sustained reactions. For these *in situ* TRXRD experi-

Table 1
Technical improvements of *in situ* time-resolved X-ray diffraction experiments which are performed to study self-sustained reactions.

System	Authors	Experiments
NiAl	Boldyrev *et al.* (1981)	Synchrotron, detector 8° (2θ), 0.5–1 s each XRD pattern
TiC, NiTi, AlNi	Wong *et al.* (1990)	Synchrotron, detector 6° (2θ), 200 ms × 200 scans
TaC, Ta_2C	Larson *et al.* (1993)	Synchrotron, detector 2 × 8° (2θ), 100 ms × 500 XRD pattern + IR thermography
	Berar *et al.* (1993)	Synchrotron, detector 17° (2θ), rapid detector
NiZr	Berar *et al.* (1994)	Synchrotron, detector 17° (2θ), 30 ms × 2000 XRD pattern
Ti–air, Ti–C, Nb–B, Ti–Si, Mo–Si,Ti–Cr–C	Merzhanov *et al.* (1995)	Conventional X-ray tube (2.5 kW), 0.5–2 s each XRD pattern
Al–Ti–Ni	Javel *et al.* (1997), Javel (1997)	Synchrotron, detector 17° (2θ), 30 ms × 2048 XRD pattern
FeAl	Gaffet *et al.* (1998)	Synchrotron, detector 17° (2θ), 180 ms × 2048 XRD pattern coupled with IR thermography
Ti_5Si_3	Kachelmeyer *et al.* (1997)	Synchrotron, detector 38° (2θ), 1 s each XRD pattern of 1024 pixels
FeAl, $MoSi_2$	Charlot *et al.* (1998)	Synchrotron, detector 17°+ 30° (2θ), 180 ms × 2048 scans coupled with IR thermography
FeAl, $FeSi_2$	Charlot, Bernard *et al.* (1999), Charlot, Gaffet *et al.* (1999), Gras *et al.* (1999)	Synchrotron, detector 30° (2θ), 50 ms × 2048 scans coupled with IR thermography

ments specific devices are used to determine the structural evolution of the SHS process. Our studies were carried out with the help of a synchrotron X-ray beam (LURE DCI-D43, Orsay, France), a fast detection system to monitor the phase transformations, and a high-temperature reaction chamber. In addition, the thermal evolution of each sample during SHS reactions was determined by means of an embedded thermocouple and an IR camera. The IR camera records the sample surface temperature, of which variation rates may reach about $+1500\ K\ s^{-1}$. In this paper we emphasize the advantages of synchrotron high-intensity radiation for studying solid-state reactions by recording simultaneously the XRD patterns (time resolution of 30 ms per pattern) with the IR sample surface images. Two examples are given. The first is a study of structural and chemical evolution during the SHS formation of NiAl intermetallics. The second is an *in situ* study of phase transformation and temperature evolution during the SHS formation of FeAl starting from mechanically activated powders.

2. Time-resolved X-ray diffraction device description

Fig. 1 describes the experimental set-up which was used to study the SHS process by TRXRD coupled to surface-temperature recording with an IR camera.

2.1. *D43 beamline characteristics*

The D43 beamline at LURE (Orsay, France) is located on the X-ray beam issuing from a synchrotron bending magnet, and consists of a curved monochromator working in the horizontal plane. The experimental set-up is located at a distance of 1.5 m from the monochromator, at its focus point, allowing users to install various kinds of experimental devices. Ge(111) or Si(111) monochromators were used to select wavelengths ranging from 0.08 nm to 0.190 nm (for example, in the case of 0.154 nm, a beam intensity of 8.9×10^9 photons $s^{-1}\ mm^{-2}$ was measured). The beam section was adjusted to ~1 × 1 mm by a collimator before the sample. Recently, a parallel-slit system has been introduced which allows the reduction of the irradiated sample zone width in the direction of the combustion front propagation in order to improve the structural resolution of the transformations. To maintain the signal-to-noise ratio at a suitable level an aperture of 200 μm (vertical) by 1.5 mm (horizontal) was chosen. This value of 200 μm leads to an irradiated zone of width ~1 mm on the sample.

2.2. *X-ray diffraction chamber characteristics*

The high-temperature chamber which has been previously developed by Javel *et al.* (1996) contains the

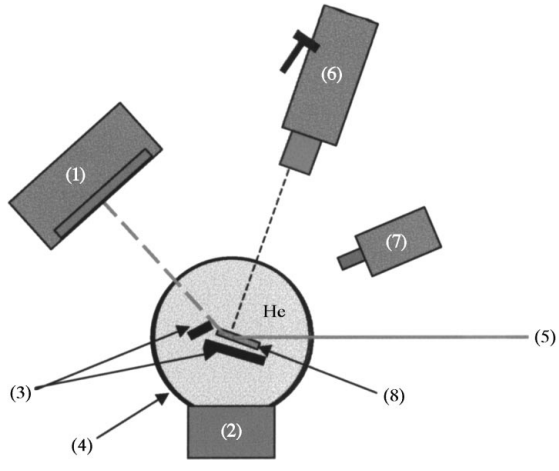

Figure 1
General view of the TRXRD experimental set-up: XRD and IR coupled devices. (1) X-ray fast detector (using 30° 2θ and 17° 2θ). (2) Reaction chamber under controlled He atmosphere. (3) Tungsten heating elements. (4) Mylar window. (5) Synchrotron radiation, λ = 0.1825 nm (LURE DCI D43, Orsay, France). (6) IR camera. (7) Video camera. (8) Sample.

sample holder with its ignition system, and works under vacuum or inert gas. The sample holder maintains the centre of the sample on the goniometer axis. During these experiments a rectangular geometry of the sample (20 × 10 mm) with a planar surface was used. The compacted samples were ignited at one end by a tungsten resistor located on the sample holder (vertical heater), while at the same time they were heated uniformly by a second heater (horizontal heater) located under the samples. The reaction chamber can work under vacuum or with various atmospheres. In our experiments all reactions were performed under helium to avoid material oxidation and to minimize gas attenuation of the incident and diffracted X-ray beams. The chamber features a 180° Mylar window for incident and diffracted X-ray beams and IR beams. It has been checked that the Mylar IR absorption does not perturb IR recording of sample images. The chamber was designed to work in reflection with an adjustable incidence angle of ~15°.

2.3. *Rapid detectors characteristics*

During the first experiments a detector designed by Berar *et al.* (1993) for rapid acquisition was used. Its beryllium window has an aperture of 120 × 6 mm. It has to be located at 400 mm from the diffracting centre and under these conditions it has an equivalent angular aperture of 17° 2θ and it may be positioned in a 180° range around the reaction chamber. Since 1997 we have used a new detector with an angular aperture of 30° 2θ which can be coupled with the first detector, thus providing an X-ray diffraction analysis on a total angular domain of 47° 2θ, split into 30° + 17.2°, with a hole of at least 26°. This improvement leads to the possibility of using a longer wavelength (0.183 nm instead of 0.099 nm) which provides expanded diffraction patterns, and helps to identify phases occurring during the front propagation. The XRD recording configuration is adjustable and we have used two different possibilities: (i) a short acquisition time, 30 ms, for individual XRD patterns, to investigate the reaction paths, but with the collection of 2048 patterns which corresponds to ~1 min of recording. Each pattern has a spatial extension of 256 channels for the 30° or 30° + 17° angular domains; (ii) a long acquisition time to define both initial and final states characterized by the collection of just two XRD patterns with an acquisition time of 30 s.

Compacted aluminium powder was used to calibrate the detection system in the 47° domain defined above, using Al lines, mainly Al(111) and Al(200). The compact was made in such a way that no preferred orientation of grains was detectable. This special feature allowed us to check the intensity response of the two detectors in the different configurations. Special care was taken to check the reproducibility of reactions in order to be able to study, if needed, a wider angular domain than 47° by changing the detector positions for two experiments with the same kind of samples.

2.4. *IR camera characteristics*

The sample temperature was recorded during the TRXRD experiments using an imaging IR camera

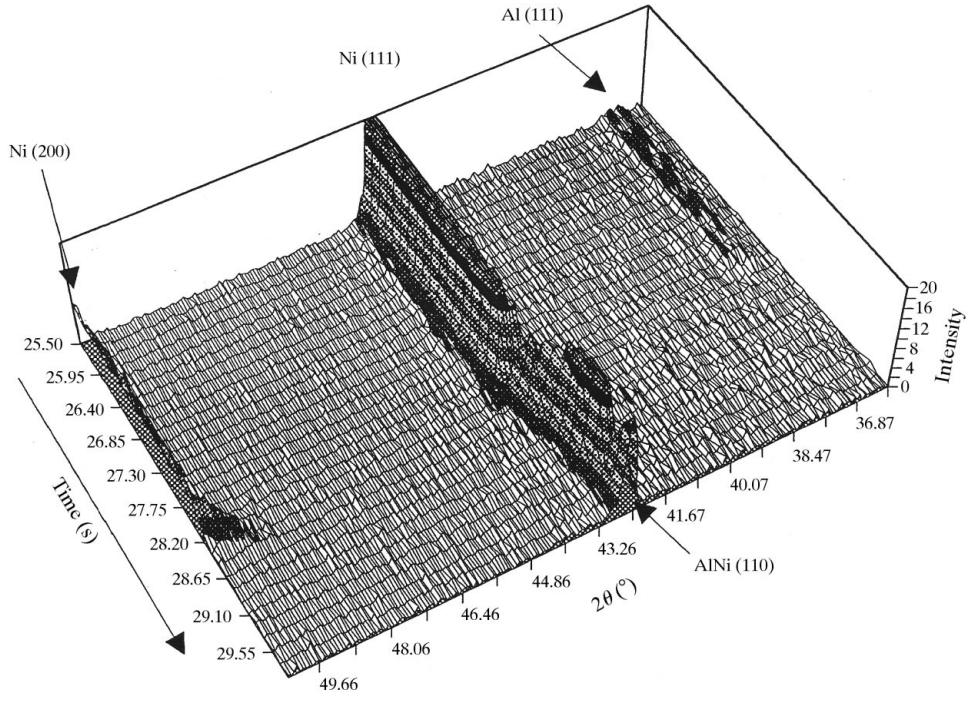

Figure 2
Combustion reaction Al + Ni = AlNi. Here, 30 patterns are shown, each being the mean of five individual patterns of 30 ms. The detector centre is at 45° from the incident X-ray beam.

(AGEMA THERMOVISION 470). This apparatus is equipped with a lens (aperture 20°) having a field of 13 × 13 cm at a distance of 0.5 m. Each pixel corresponds to a sample area of 1 × 1 mm. Thermal images were continuously recorded at a fixed rate of five images per second with the camera and a U-matic video recorder. The Mylar window of the chamber is transparent in the wavelength range where the IR camera operates (2–5 μm). The main difficulty with this equipment is to determine the sample emissivity which changes during the reaction. Emissivity values are determined before and after combustion and an interpolated value is taken for the reaction period. The validity of such interpolations may be tested in some cases when the reaction course goes into a 'thermostat' mode at a well known temperature, such as in aluminium fusion.

2.5. *XRD–IR synchronization*

It is essential to obtain a synchronization of the XRD patterns and IR images. Using a fluorescent paper featuring the sample size, the X-ray spot was located and recorded by video camera. After the analysis of this image, the coordinates of the irradiated area were defined and translated into pixel numbers of the IR image.

The only way to perform the synchronization was to locate the commencement of X-ray acquisition on the corresponding IR image. This was performed with an incandescent lamp, placed in the camera field, which was switched on simultaneously with the XRD collection.

3. Experimental details and results

3.1. *TRXRD study of NiAl formation by SHS*

The binary intermetallics of the Al–Ni system have characteristics which make them candidates for high-temperature structural applications. Unfortunately, their lack of ductility is such that their practical use is not yet widely spread. Different ways have been explored to cure their room-temperature brittleness and to improve their creep properties at high temperatures. At the same time their synthesis by SHS may be considered as a very attractive process since its energy consumption would be small and the control of the synthesis could help to reduce the mechanical problems. This is the reason why we started with a study of the reaction $x\mathrm{Ni} + y\mathrm{Al} = \mathrm{Ni}_x\mathrm{Al}_y$ by TRXRD.

3.1.1. *Experimental conditions*. Fine powders of the two metals (typically −325 mesh, 99.5 wt% pure) were mixed in the correct proportion for AlNi in a glove box under purified argon, together with 20% vol. of alumina (used as a heat sink), and compacted in a steel die under a pressure of $\sim 6 \times 10^8$ Pa. The compacts were 2 cm × 1 cm × 2–3 mm. Thermocouples were embedded inside the compacts in order to monitor their temperature. The addition of alumina was necessary to keep the sample surface flat during the SHS process as the enthalpy of reaction is high enough in these experimental conditions to melt the product. It has to be mentioned that, even at such a concentration, alumina lines are seldom observed on the diffraction patterns: they are only detected from time to time when the displacements due to thermal expansion and contraction bring a grain into a favourable diffraction position. The TRXRD conditions were as follows: the acquisition time for one pattern was fixed at 30 ms and the number of patterns at 2048, which corresponds roughly to 1 min of recording. The 30° detector position was at 45° or 39° from the incident X-ray beam direction in order to show Ni(111) and Ni(200) when at 45° or Ni(111) and Al(111) at 39°, with a wavelength of 0.1545 nm. The 30° angular domain was divided into 256 channels.

3.1.2. *Experimental results*. The reaction between aluminium and nickel is initiated by heating the sample uniformly by first the horizontal heater then at one end by the vertical heater. At first, aluminium fusion propagates from the heated end through the sample and a corresponding red wave (∼933 K) may be seen and recorded. Following this, a second wave, emitting in the yellow range (∼1473–1673 K), indicates that the reaction of formation is taking place. TRXRD (Fig. 2) shows first a steady state for nickel during the melting of aluminium which provides a thermostat, followed by a sudden increase of the nickel temperature as the Al lines disappear. The Ni temperature may be deduced from its cell parameter expansion and linear expansion coefficients. The maximum value obtained is ∼1673 K. At this temperature only nickel and AlNi remain solid. Nickel line intensities decrease as liquid aluminium begins to surround the Ni grains, soon after melting, but the reaction between Al and Ni is slow at the aluminium melting point. As the temperature of the sample at the heated end increases sharply, both by electric and reaction heating, the reaction rate also increases and the second thermal wave crosses the sample. The Ni temperature may be estimated as higher than 1273 K before the Ni lines decrease in intensity indicating that the AlNi quantity has become noticeable. The AlNi(110) peak is almost at the same position as Ni(111) but the Ni(200) peak is isolated and it is therefore possible to locate its disappearance. At the same time the AlNi(110) peak begins to grow and is shifted to lower angles (the compound temperature is slightly increased) and then it moves slowly towards higher angles when the temperature falls behind the reaction front. Under the experimental conditions here the temperature jump from the aluminium melting point to the disappearance of Ni(200), which corresponds to the formation of a layer of product thick enough to hide the remaining nickel, lasts for 0.9 s and the temperature begins to fall 1.05 s later when the reaction front is far enough to allow the cooling of the X-ray irradiated zone. Several observations have been made on AlNi and they show that the commencement of reaction between Al and Ni does not correspond to the end of aluminium melting. At the end of the aluminium melting the consecutive jump of temperature is mainly due to the fact that there is nothing left to fix the temperature at ∼933 K but that most of the reaction

heat is produced later, at ~1273 K or more, when the reaction kinetics are enhanced by the arrival of the second thermal wave. The interference between the sample heat conductivity which governs the temperature profile and the reaction kinetics which control the heat release provides a good example of the value of correlating TRXRD and IR imaging.

3.2. *TRXRD study of FeAl intermetallics MASHS formation*

Although iron aluminides exhibit lower densities than steels and good high-temperature properties, their mechanical uses are limited due to brittle fracture and low ductility at room temperature (Takasugi *et al.*, 1987; Wang *et al.*, 1990). One solution to this is to decrease the crystallite size. However, conventional processes do not lead to nanostructured materials. Previous work has shown that mechanically activated self-propagating high-temperature synthesis (MASHS) applied to the case of the Fe–Al system maintains the nanostructure, induced by previous ball-milling during and after the combustion reaction (Charlot, Bernard *et al.*, 1999). In addition, other experiments have been successfully carried out on Fe–Si (Gras *et al.*, 1999) and Mo–Si (Charlot *et al.*, 1998) systems.

3.2.1. *Experimental conditions*. MASHS is mainly the combination of two steps. The first step is a mechanical activation where pure elemental powders (Fe + Al) are milled together inside a planetary mill for a short time at a given shock energy and frequency. The short period of milling is carried out using the high-energy planetary machine, denoted G5, which allows shock frequency and shock energy to be chosen independently (Gaffet, 1991). The physical parameters (Abdellaoui & Gaffet, 1995) of the planetary milling machine are as follows: the vials are fixed onto a rotating disc (rotation speed Ω) and rotate in the opposite direction to the disc with a speed ω. The values of Ω (150 r.p.m.) and ω (200 r.p.m.) were checked and controlled by an ultrasonic tachometer. The duration of the milling process is 4 h in order to avoid the formation of some intermetallic fractions, and to allow the formation of a nanoscaled chemical gradient. Indeed, the mechanical activation leads to the formation of micrometre-sized powders, which contain nanoscaled three-dimensional polyinterfaces of the elemental compound (Abdellaoui & Gaffet, 1995; Gaffet & Tillement, 1997; Gaffet *et al.*, 1999). After extraction from the milling vials the mechanically activated particles were compacted like the mixtures of Al and Ni powders (§3.1) but without the addition of a heat sink.

The second step, an SHS reaction, uses the exothermicity of the Fe + Al reaction. *In situ* time-resolved experiments were performed under the following conditions: the wavelength was set to 0.183 nm, the aperture of the parallel slit was 200 µm × 1.5 mm, and the 30° (2θ) rapid detector was centred at 55° (2θ) to collect simultaneously the Al(111), Fe(110) and Al(200) peaks, and FeAl(110), the most intense peak of the end product. The 17° (2θ) rapid detector was centred at 102° (2θ) to collect simultaneously Al(311), Fe(211), Al(222) and FeAl(211). The time of each X-ray acquisition was 50 ms during 102.4 s which corresponds to 2048 scans per experiment; the sample surface IR image was taken every 200 ms.

3.2.2. *Experimental results*. A transitory phase is observed during the FeAl MASHS as shown in Fig. 3. In this figure one can observe the first XRD patterns recorded just before the reaction ignition, and that the

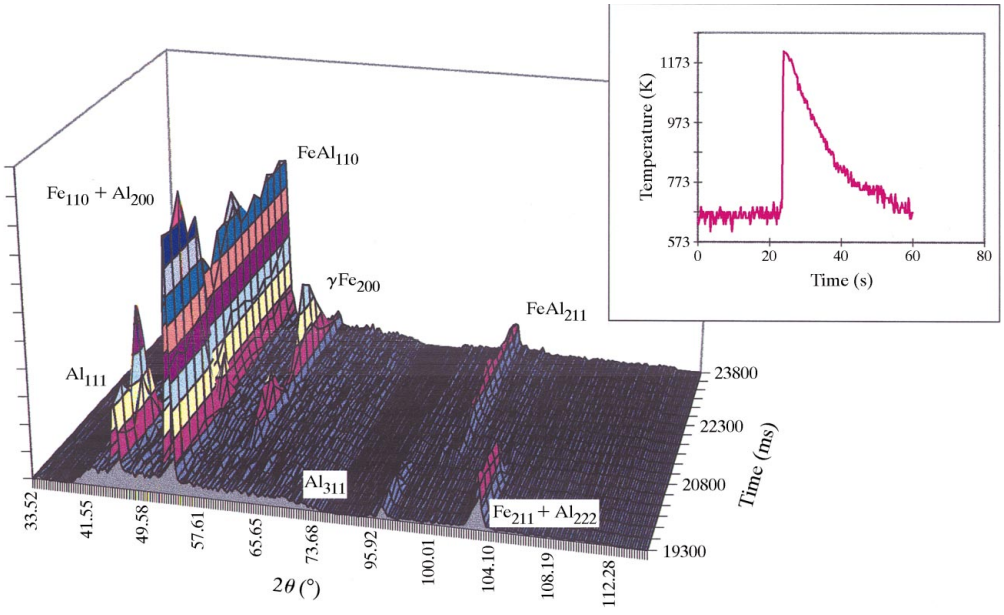

Figure 3
In situ TRXRD MASHS reaction Al + Fe = FeAl. Here, 20 patterns are shown, each being the mean of five individual patterns of 30 ms. On the right-hand side a typical IR thermogram after an analysis on a single pixel in the irradiated area is represented.

Al(111) intensity increases and is then reduced to zero. This may be due to a reorganization of solid aluminium in the temperature range close to 723 K and subsequent melting. Then, as the combustion wave propagates inside the irradiated area, the FeAl intermetallic phase grows. At 23.7 s, when the combustion wave passes through the diffracted area (whose temperature is ~1023–1123 K), the Fe(110) and Al(200) intensities decrease and the FeAl(110) peak appears. Simultaneously, a transitory peak appears and disappears. At the end of this SHS reaction, only FeAl is detected by XRD. The transitory phase is only observed for 3 s. A search for this phase shows that it is neither an intermetallic compound of the Fe–Al system (FeAl, Fe_2Al_5, $FeAl_2$, . . .) nor an Fe–Al–O compound or oxide (the experiment was performed in a helium flux). The two peaks observed at 20.6 s are located at positions corresponding to a face-centred cubic system with a lattice parameter ~0.36 nm. These observations suggest that the transitory phase is γFe. It appears close to 1173 K (IR analysis), this value being in agreement with the known transition temperature, 1183 K (Massalski *et al.*, 1990), for the αFe to γFe transition.

Under the experimental conditions here the reaction heat is sufficient to increase the temperature of the reacting medium up to the transition point between αFe and γFe and to induce this transition, but, as soon as γFe appears, the reaction rate with Al is reduced because the solubility of Al in γFe is limited and the synthesis of FeAl requires another structural transformation. The reduction in reaction rate limits the quantity of heat released so that the Fe reverts back to the α phase and allows the reaction to proceed again at a faster rate. This mechanism stabilizes the reaction front temperature at ~1123 K and probably helps to maintain the grain size at the nanometre scale since grain growth cannot be effective at such temperatures and short periods. One can therefore conclude with certainty that a full elucidation of the reaction path from elemental powders to FeAl intermetallics by MASHS techniques requires complementary experimentation with TRXRD. Further improvements of the quality of diffractograms would be achieved by the spatial resolution of the detectors.

4. Conclusions

This paper shows how it is possible to analyse a solid–solid or solid–liquid reaction by TRXRD coupled with IR imaging. Two different compound formations have been described: AlNi and AlFe. It has been shown that a new insight into the reactions may be achieved by using synchrotron radiation. In the case of AlNi the different steps of reaction, aluminium melting, subsequent temperature increase and fast reaction between Al and Ni, at such a temperature that only Ni and AlNi are solid and all other compositions are liquid, are well identified. The formation of FeAl during an MASHS leads to the observation by TRXRD of an original phenomenon. Indeed, a fraction of the iron appears to transform into its γ allotropic phase and this transition stabilizes the reaction temperature at ~1123 K. In addition, the observed aluminium melting during the reaction explains why the nanostructure induced by the mechanical activation is maintained in the end product.

The authors gratefully acknowledge M. Bessiere (LURE CNRS), J. F. Berar (ESRF CNRS), J. Doucet (LURE CNRS), J. F. Javel, O. Held (CNRS, University Nancy), F. Charlot, C. Gras, J. C. Niepce (CNRS, Université de Bourgogne) for their valuable help during the experiments. The authors specially acknowledge V. Mathae for his assistance and help with the thermal analysis.

References

Abdellaoui, M. & Gaffet, E. (1995). *Acta Mater.* **43**(3), 1087–1098.

Berar, J. F., Javel, J. F., Dirand, M. & Gachon, J. C. (1994). *First European Conference on Synchrotron Radiation in Materials Science*, Chester, UK, 3–8 July 1994, Poster 5.A3.

Berar, J. F., Lemmonier, M., Bartol, F., Grammond, M. & Chevreul, J. (1993). *Nucl. Instrum. Methods Phys. Res. B*, **82**, 146–150.

Boldyrev, V. V., Aleksandrov, V. V., Tolochko, M. A., Gusenko, S. N., Sokolov, A. S., Sheronov, M. A. & Lyakhov, N. Z. (1981). *Combust. Explos. Shock Waves (USSR)*, **259**(5), 722–725.

Charlot, F., Bernard, F., Gaffet, E. & Niepce, J. C. (1999). *Acta Metall.* **47**, 619–629.

Charlot, F., Gaffet, E., Bernard, F., Zeghmati, B. & Niepce, J. C. (1999). *Mater. Sci. Eng. A*, **262**, 279–288.

Charlot, F., Gras, Ch., Gramond, M., Gaffet, E., Bernard, F. & Niepce, J. C. (1998). *J. Phys IV*, **C8**(5), 497–504.

Gaffet, E. (1991). *Mater. Sci. Eng. A*, **135**, 291–293.

Gaffet, E., Bernard, F., Niepce, J. C., Charlot, F., Gras, Ch., Le Caer, G., Guichard, J. L., Delcroix, P., Mocellin, A. & Tillement, O. (1999). *J. Mater. Chem.* **9**, 305–314.

Gaffet, E., Charlot, F., Bernard, F., Klein, D. & Niepce, J. C. (1998). *Mater. Sci. Forum*, **269/272**, 379–384.

Gaffet, E. & Tillement, O. (1997). *Ann. Chim.* **22,** 417–422.

Gras, Ch., Gaffet, E., Bernard, F. & Niepce, J. C. (1999). *Mater. Sci. Eng. A*, **264**, 94–107.

Javel, J. F. (1997). Thesis, University Henri Poincaré, Nancy 1, France.

Javel, J. F., Dirand, M., Kuntz, J. J., Nazzik, F. Z. & Gachon, J. C. (1997). *J. Alloy Compd.* **247**, 72–81.

Javel, J. F., Dirand, M., Nazzik, F. Z. & Gachon, J. C. (1996). *J. Phys IV*, C**2**(6), 229–234.

Kachelmeyer, C. R., Khomenko, I. O., Rogachev, A. S. & Varma, A. (1997). *J. Mater. Res.* **12**(12), 3230–3240.

Larson, E. M., Wong, J., Holt, J. B., Waide, P. A., Nutt, G., Rupp, B. & Treminello, L. J. (1993). *J. Mater. Res.* **8**(7), 1533–1541.

Massalski, T. B., Okamoto, H., Subramanian, P. R. & Kacprzak, L. (1990). *Binary Alloy Phase Diagrams*, Vol. 1, 2nd ed. Ohio: ASM International.

Merzhanov, A. G. & Borovinskaya, I. P. (1972). *Dokl. Akad. Nauk. SSSR*, **204**(2), 366–369.
Merzhanov, A. G., Borovinskaya, I. P., Khomeko, I. O., Mukasyan, A. S., Ponomarev, V. I., Rogashev, A. S. & Shkiro, V. M. (1995). *Ann. Chim. Fr.* **20**, 123–138.
Munir, Z. A. (1988). *Ceram. Bull.* **67**(2), 342–349.
Takasugi, T., Masahashi, N. & Izumi, N. A. (1987). *Acta. Metall.* **35**, 381–390.
Wang, K., Nishikata, A., Shinoda, D. & Suzuki, T. (1990). *Z. Metallkd.* **81**, 581–585.
Wong, J., Larson, E. M., Holt, J. B., Waide, P. A., Rupp, B. & Frahm, R. (1990). *Science*, **249**, 1406–1409.